

RELAXATION METHOD FOR NAVIER–STOKES EQUATION

P. M. C. DE OLIVEIRA

*Instituto de Física, Universidade Federal Fluminense
Av. Litorânea s/n, Boa Viagem, Niterói 24210-340, RJ, Brazil
National Institute of Science and Technology for Complex Systems, Brazil
pmco@if.uff.br*

Received 25 August 2011
Accepted 21 February 2012
Published 25 April 2012

The motivation for this work was a simple experiment [P. M. C. de Oliveira, S. Moss de Oliveira, F. A. Pereira and J. C. Sartorelli, preprint (2010), arXiv:1005.4086], where a little polystyrene ball is released falling in air. The interesting observation is a speed breaking. After an initial nearly linear time-dependence, the ball speed reaches a maximum value. After this, the speed finally decreases until its final, limit value. The provided explanation is related to the so-called *von Kármán street* of vortices successively formed behind the falling ball. After completely formed, the whole street extends for some hundred diameters. However, before a certain transient time needed to reach this steady-state, the street is shorter and the drag force is relatively reduced. Thus, at the beginning of the fall, a small and light ball may reach a speed superior to the sustainable steady-state value.

Besides the real experiment, the numerical simulation of a related theoretical problem is also performed. A cylinder (instead of a 3D ball, thus reducing the effective dimension to 2) is positioned at rest inside a wind tunnel initially switched off. Suddenly, at $t = 0$ it is switched on with a constant and uniform wind velocity \vec{V} far from the cylinder and perpendicular to it. This is the first boundary condition. The second is the cylinder surface, where the wind velocity is null. In between these two boundaries, the velocity field is determined by solving the Navier–Stokes equation, as a function of time. For that, the initial condition is taken as the known Stokes laminar limit $V \rightarrow 0$, since initially the tunnel is switched off. The numerical method adopted in this task is the object of the current text.

Keywords: Turbulence; Navier-Stokes equation.

1. Introduction

Relaxation is the prime numerical method to solve Laplace equation $\nabla^2\psi(\vec{r}) = 0$ for a field $\psi(\vec{r})$ inside a surface where some fixed boundary condition is defined. It is based on the fact that $\psi(\vec{r}_o)$ equals the continuous average over neighboring values along a closed contour around \vec{r}_o . Translated to a discrete mesh (for instance a square or cubic lattice), $\psi(\vec{r}_o)$ should be equal to the discrete average over the neighboring lattice points. The method consists in starting from some trial distribution of $\psi(\vec{r})$ over the lattice points inside the region of interest, which does not obey the quoted

average rule. Then, each $\psi(\vec{r})$ is replaced by the average over its neighbors, sequentially, up to numerical convergence over the whole region. For a good description of this traditional and simple method, see Ref. 1.

The relaxation idea can be extended to other problems, more complicated than the Laplace one, by profiting from the same property of the Laplacian operator ∇^2 . For instance, the Navier–Stokes equations for incompressible fluid dynamics can be written as in the forthcoming Eqs. (1)–(3), introduced in Ref. 2. This particular formulation, based on the so-called vorticity field $\vec{\omega}$ instead of the velocity field \vec{v} , is convenient because the Laplacian operator acts on $\vec{\omega}$, not on \vec{v} . The purpose of this work is to explore this idea.

Relaxation methods are historically applied to the traditional formulation of the Navier–Stokes equation (based on the field \vec{v} , not in $\vec{\omega}$), mainly by engineers not by physicists, see for instance Ref. 3. The reason for that is presumably the practical interest in aeronautics and similar research fields. During the last half century, many sophisticated improvements have been introduced in order to enhance the performance of the numerical task. Examples are: The division of matrices into convective and viscous parts; curved mesh according to the geometry of the fixed object crossed by the fluid, with lines orthogonal to the surface of this object; nonuniform mesh with smaller cells near the object; methods for implementing the routines in many processors in parallel, etc. None of these improvements are implemented here, the purpose is just to test the direct relaxation of the vorticity $\vec{\omega}$ instead of \vec{v} , an idea which has not yet been explored, at least up to my knowledge. Performance improvements are postponed.

Figure 1 shows the result of a home made experiment.⁴ A polystyrene ball with diameter $D = 2.5$ cm and mass of 0.2 g is released from different heights above the floor and the falling time is measured with a hand chronometer.

A Reynolds number $\mathcal{R} \approx 6000$ is reached at the end of the fall (speed $V \approx 4$ m/s).^a In this regime, the steady-state drag force is experimentally known to be proportional to the squared speed. This is certainly true at the end of the fall some 3 m below the release point. However, just after the first centimeter of fall the Reynolds number is already $\mathcal{R} \approx 1000$, entering into the range ($10^3 < \mathcal{R} < 10^5$) where the proportionality (drag force *vs* squared speed) holds. Therefore, by neglecting the first centimeter of a much longer fall, it seems legitimate to adopt this proportionality during the whole fall. However, the result of this approach is the lower curve in Fig. 1, in clear disagreement with reality.

The mistake is to adopt a *distance* limit, 1 cm, as the standard for neglecting what occurred before the steady-state regime is reached. Instead, one should adopt a *time* limit as the standard for the transient to be taken into account. Figure 1 again leads to the conclusion that the drag force is negligible (compared with the ball’s weight) before the first half second of the fall, since the two leftmost experimental points coincide with the free fall parabola. Note the speed at that time already larger than

^a $\mathcal{R} = VD/\nu$, where $\nu \approx 1.7 \times 10^{-5}$ m²/s is the air ratio viscosity/density.

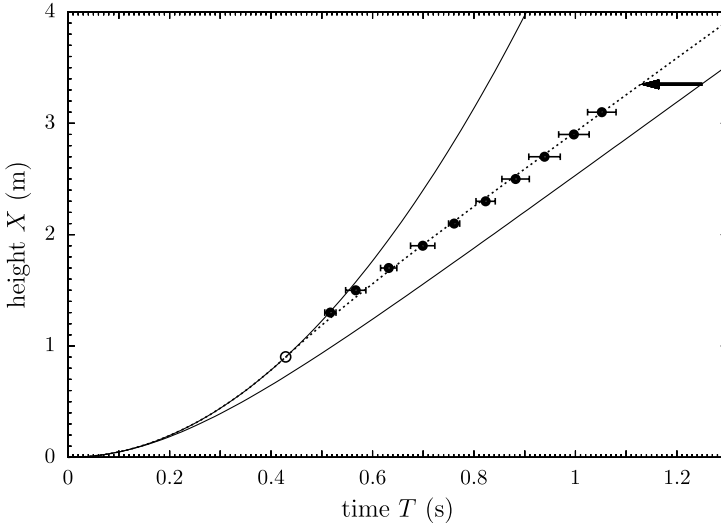


Fig. 1. Falling time for different heights. The vertical error bars are negligible. The horizontal error bar displayed for each experimental point is calculated from the statistics of 10 repeated time measurements. Using the Earth gravitational field $g = 9.8 \text{ m/s}^2$, the upper curve is the free fall parabola, $X = gT^2/2$, no friction at all. The other two curves correspond to a friction force proportional to the square of the speed. At the lower curve, this force acts during the whole fall, since beginning. At the intermediate, dotted curve, the same force is switched on *only after* an adjusted initial transient time (open bullet), with no friction before that. Note that the slope of this curve has a maximum around $\approx 0.4 \text{ s}$. Note also that the observed fall is in advance by more than 0.1 s (arrow), relative to the lower curve.

the final steady-state value, as a closer look to the slopes between successive experimental points in the figure shows. The Reynolds number reaches its maximum of some ten thousands. The overall conclusion is that, during a transient of half a second, i.e. before the first meter of fall, the drag force is indeed much smaller than the steady-state value predicted for this range of Reynolds numbers.

The dotted line in Fig. 1 was obtained by the simple procedure of neglecting the drag force before an adjusted transient time, with the squared speed rule after that. It is adjusted to 0.42 s in order to fit just the rightmost experimental point. In doing so, the other points result also fitted, as well as the final speed (slope). A second version of the experiment was performed⁴ by observing successive snapshots of the fall, obtained with a fast camera. With this device the speeds could be precisely measured. The surprising effect of losing speed is indeed confirmed.

The conceptual explanation for the phenomenon comes from the gradual formation of successive turbulent vortices behind the ball, the so-called von Kármán street responsible for the drag force proportional to the square of the speed. Looking from the reference frame of the ball, each vortex is formed close to it and goes away with a small speed, much smaller than the wind speed. Soon, another vortex is formed, following the same fate and so on successively. Looking from the lab reference frame, the successive vortices run down behind the ball almost with the same

speed, i.e. they are dragged by the ball. Indeed, the street of vortices is experimentally known to extend for some hundred diameters behind the ball, corresponding in our case to the order of magnitude of a meter. Therefore, only after the ball has already fallen approximately 1 m the vortices street is completely formed. Before that, the drag force is much smaller, similar to the Stokes laminar regime proportional to the (nonsquared) speed, negligible in the present experimental case. While still under this reduced drag force during the beginning of the fall, the ball reaches a speed larger than its own future limit value which is settled only after the vortices street is completely formed.

The current text is organized as follows. Next section describes a related theoretical problem to be solved numerically: A cylinder is fixed inside a wind tunnel initially switched off, $\mathcal{R} = 0$, when the wind is suddenly switched on at time $t = 0$ according to a larger and constant Reynolds number, say $\mathcal{R} = 30$ or $\mathcal{R} = 1000$. This is not exactly the same problem of the experiment, where the Reynolds number gradually increases as the ball accelerates. Also the ball is replaced by a cylinder perpendicular to the wind in order to reduce the computer effort from 3D to 2D. In spite of these differences, this new theoretical problem shares with the experiment the transient behavior of gradual formation of the von Kármán vortices street. It allows us to observe the evolving air velocity flow around the cylinder, during this transient. A relaxation method for the numerical solution of Navier–Stokes equation is introduced and applied to this problem. Finally, conclusions are presented in the last section.

2. Relaxation Method for Navier–Stokes

In principle one can theoretically approach the experimental problem described in the previous section by some phenomenological relation providing the drag force as a function of the speed *and time* and then solving Newton's law by adding this force to the weight of the ball. The important point is to realize that the drag force cannot be a function of the speed only, some explicit time dependence should hold during the transient at the beginning of the fall. One can invent a lot of such phenomenological approaches, by including retarded terms into known formulas, or obtaining them from linear approximations (see Ref. 5), or other complications. In all of them, during the transient initial time, the steady-state already known value must be replaced by something else much smaller. The simplest approach is to neglect this “something else” completely, no drag at all during the transient. This procedure was already performed in the intermediate curve of Fig. 1, where a transient time of 0.42 s is adjusted in order to fit the rightmost experimental point. The problem can be solved even analytically.⁶

None of these phenomenological, macroscopic approaches would be helpful in understanding what is going on concerning the air flow behind the ball, which indeed is the ultimate phenomenon responsible for the macroscopic observations. Therefore, in order to study the phenomenon, one needs to adopt some approach allowing to

define local air velocities around the ball, within a mesoscopic, sub-millimetric scale. In other words, one needs to face the solution of the Navier–Stokes nonlinear equation, a much harder numerical problem.

This is not a trivial task for the falling ball case. A time-dependent Reynolds number $\mathcal{R}(t)$ must be calculated “on flight”, starting from $\mathcal{R}(t = 0) = 0$ when the ball is released. Worse, in order to know the function $\mathcal{R}(t)$ one needs to calculate the drag force at each time, which added to the ball’s weight allows one to determine the instantaneous speed variation. From that, the current speed can be obtained by integration since $t = 0$ and hence $\mathcal{R}(t)$. The determination of the drag force from the current velocity field around the ball is traditionally obtained from the velocity field gradient at the ball surface. Therefore, one needs high precision to pick up a 2D surface which corresponds to a null-measure set inside a 3D field.^b

Instead of this hard numerical problem, we decided in Ref. 4 to simplify it along two directions. First, the ball is replaced by a long cylinder (direction Z) at rest perpendicular to the wind (direction X). In addition, the air flow around is also supposed to be perpendicular to the cylinder, i.e. a 2D velocity field on the XY plane. Experiments justify these assumptions. The known curves for the steady-state drag force on a sphere or on such a cylinder are essentially the same. Moreover, the observed velocity field indeed remains restricted to planes perpendicular to the cylinder, within the range of Reynolds numbers we are dealing with.

Second simplification, the unknown function $\mathcal{R}(t)$ is replaced by a simple step function

$$\mathcal{R}(t) = \begin{cases} 0, & t \leq 0, \\ \mathcal{R}, & t > 0, \end{cases}$$

where \mathcal{R} is some constant.^c The initial velocity field adopted at $t = 0$ is the laminar Stokes configuration which holds for a vanishing Reynolds number. Then, vortices are initially absent, but will be gradually formed as time goes by. One can thus observe the transient regime of interest, in particular one can observe the transient time elapsed until the complete formation of the von Kármán street. As a result obtained from the numerical solution described below, the estimated transient time corresponds to a wind travelled distance of some half-hundred diameters at least. It is certainly smaller than the real one observed in the falling ball experiment, since an already large \mathcal{R} is set since $t = 0$, in contrast with the ball case where $\mathcal{R}(t)$ slowly increases. This result is therefore compatible with the provided explanation⁴ for the

^b A possible trick to bypass this difficulty is to remove the ball and repeat the calculation of the velocity field at $t + dt$ from the known configuration at t with the ball. Removed the ball at t , the velocity field is allowed to penetrate a little bit inside the volume the ball would occupy. Then, by integrating the penetrating velocities inside this volume one gets the total momentum which would be transferred to the ball from the air around. Dividing this momentum by dt one gets the instantaneous drag force. This procedure is entirely 3D, reducing the necessity of too high precision near the ball surface.

^c The drag force can be obtained analytically in the limit of low \mathcal{R} , see problem 9 of Ref. 5. Curiously, the resulting force also decays with time as in our experiment. However, our interest is the case of large \mathcal{R} where the vortices street appears and no analytical formulas are available.

breaking during the fall, since the observed von Kármán street indeed extends for some hundred diameters downstream.

Already taken in dimensionless units,² the Navier–Stokes equation is

$$\frac{\partial \vec{\omega}}{\partial t} = \frac{1}{\mathcal{R}} \nabla^2 \vec{\omega} - \vec{\nabla} \times (\vec{\omega} \times \vec{v}), \quad (1)$$

where \vec{v} are the air velocities in different positions. In our 2D case, one has $\vec{v}(x, y, t) = v_x(x, y, t)\hat{x} + v_y(x, y, t)\hat{y}$. The vorticities

$$\vec{\omega} = \vec{\nabla} \times \vec{v} \quad (2)$$

are auxiliary vectors. In our case they are always parallel to the cylinder, i.e. they represent a scalar field $\omega(x, y, t)$. Additionally, air density fluctuations do not appear in our experiment because all speeds are much smaller than the sound speed (≈ 330 m/s). Therefore we can set

$$\vec{\nabla} \cdot \vec{v} = 0. \quad (3)$$

The set of Eqs. (1)–(3) completely define the problem. Two boundary conditions are adopted: (I) null velocities and vorticities along the cylinder surface as well as inside it; and (II) wind velocity $\vec{v} = V\hat{x}$ and null vorticities far from it. Here, $V = 1$ in the dimensionless units all equations above are already expressed. Given some initial field $\vec{v}(x, y, t = 0)$, one can solve the set (1)–(3) in order to obtain the velocities at any position (x, y) in any time $t > 0$.

Let’s start with the Stokes laminar limit for which the Navier–Stokes equation reduces to the Laplace equation

$$\nabla^2 \omega = 0 \quad \text{for } \mathcal{R} \rightarrow 0 \quad (4)$$

which must be solved inside the outer boundary (rectangle) and outside the inner boundary (circle) displayed in Fig. 2. Note that in this Stokes limit the flow is stationary, no time dependence.

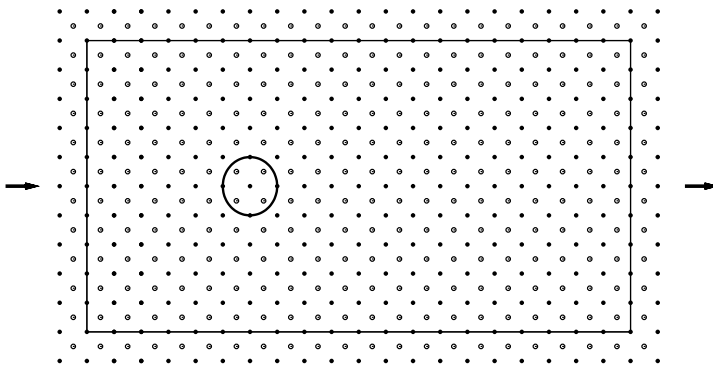
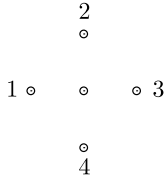
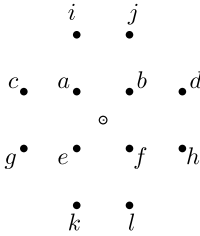


Fig. 2. Square grid adopted in the numerical solution. The inner circle represents the cylinder, inside which the velocities are kept null. Outside the rectangle, velocities are kept equal to the fixed wind velocity indicated by the arrows. In between, the velocities \vec{v} are defined at the full dots, whereas the vorticities ω at the open bullets. Only few points are represented for clarity, the real grid has 400×200 full dots inside the rectangle.



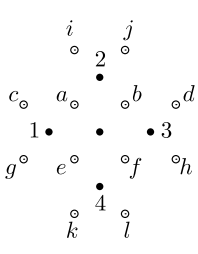
$$\omega = \frac{1}{4}(\omega_1 + \omega_2 + \omega_3 + \omega_4) \quad (5)$$

Fig. 3. Relaxation method. The value of ω at the central point is replaced by the average over its neighbors, Eq. (5).



$$\omega = \frac{1}{16\Delta} \left[9 \left(-v_{xa} - v_{xb} + v_{xe} + v_{xf} - v_{ya} + v_{yb} - v_{ye} + v_{yf} \right) + v_{xc} + v_{xd} - v_{xg} - v_{xh} + v_{yi} + v_{yj} - v_{yk} - v_{yl} \right] \quad (6)$$

Fig. 4. Translator $\vec{v} \Rightarrow \omega$. The value of ω at the central open bullet is given by Eq. (6), where x and y refer to directions, while $a, b \dots l$ refer to the neighboring points indicated in the figure. The extended two-shells neighborhood is adopted in order to retain (at least) second-order accuracy relative to the first-neighbor distance Δ (in the current implementation, $\Delta = 0.025$).



$$\begin{aligned} v_x &= \frac{1}{4} (v_{x1} + v_{x2} + v_{x3} + v_{x4}) \\ &\quad - \frac{\Delta}{64} [9 (-\omega_a - \omega_b + \omega_e + \omega_f) + \omega_c + \omega_d - \omega_g - \omega_h] \\ v_y &= \frac{1}{4} (v_{y1} + v_{y2} + v_{y3} + v_{y4}) \\ &\quad - \frac{\Delta}{64} [9 (-\omega_a + \omega_b - \omega_e + \omega_f) + \omega_i - \omega_j + \omega_k - \omega_l] \end{aligned} \quad (7)$$

Fig. 5. Translator $\omega \Rightarrow \vec{v}$. The values of v_x and v_y at the central point are given by Eq (7). Both should be applied many times to all points, with fixed ω , until convergence.

Equation (4) can be numerically solved by the traditional relaxation method¹ illustrated in Fig. 3. The procedure should be repeated for all points, in any chosen order, again and again until convergence. In our case, however, \vec{v} is also present, not only ω , therefore a translator $\vec{v} \Leftrightarrow \omega$ is needed. It is defined in Figs. 4 and 5. As boundary conditions, $\vec{v} = \hat{x}$ is imposed at all full dots along the rectangle of Fig. 2, and also outside it, as well as $\omega = 0$ at the external open bullets. Along the circular line and inside it, $\vec{v} = \omega = 0$.

Equation (6) is simply the discretized version of Eq. (2). It is second-order accurate in the grid spacing Δ , a very important care we kept along all our numerical

procedure. Long range correlations are expected to occur, say within a macroscopic scale $L = N\Delta$ where N is a large number. In order to properly link two points distant L from each other, one needs to jump some N steps on the grid in going from one point until the other, accumulating the numerical errors in each step, i.e. multiplying the local inaccuracy by $N = L/\Delta$. Therefore, with a second-order local inaccuracy proportional to Δ^2 , the total error remains controllable, i.e. proportional to Δ . Any desired accuracy can thus be obtained simply by taking a small enough Δ . Equations (7) mixes (2) and (3), allowing to obtain the vector field \vec{v} from the knowledge of its curl and divergence.

In order to solve the Stokes Eq. (4) one starts from some velocity distribution respecting the boundary conditions. For example all velocities $\vec{v} = \hat{x}$ outside the cylinder and null inside. From that, one determines ω through Eq. (6) at every grid point (open bullets). Then, ω is relaxed through Eq. (5), over the whole grid, repeating this procedure as many times as needed until convergence. Finally, a new \vec{v} distribution is determined through Eq. (7), this step being also repeated until convergence. The resulting ω distribution is shown in Fig. 6. The streamlines, in Fig. 7.

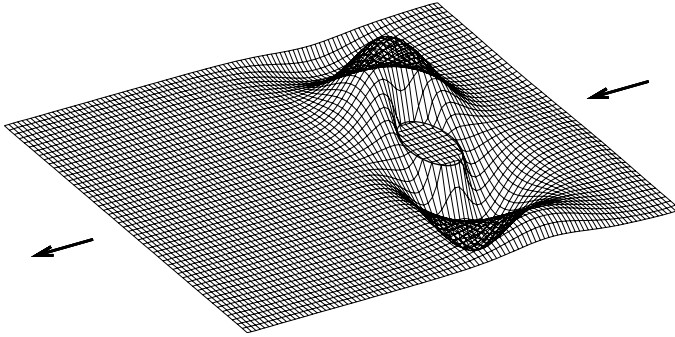


Fig. 6. Stokes configuration ($\mathcal{R} \rightarrow 0$), vorticity $\omega(x, y)$.

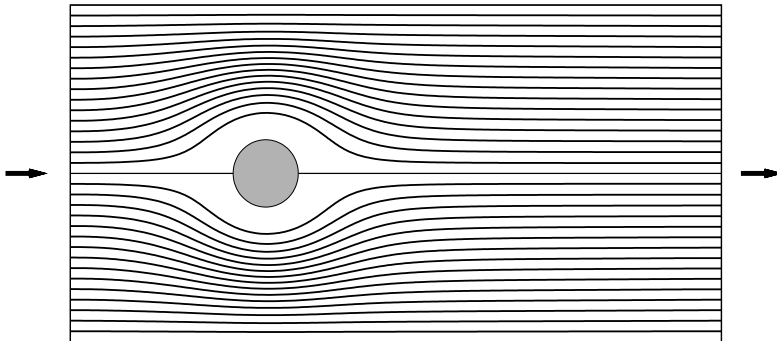


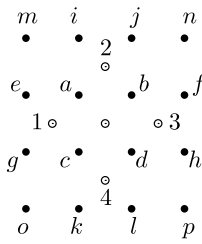
Fig. 7. Stokes configuration ($\mathcal{R} \rightarrow 0$), streamlines. The velocity $\vec{v}(x, y)$ is tangent to these lines at each point.

Considering the origin at the cylinder center, the $\mathcal{R} \rightarrow 0$ time-independent Stokes configuration shown in Figs. 6 and 7 presents two symmetries, relative to both axis X and Y

$$v_x(x, -y) = v_x(x, y), \quad v_y(x, -y) = -v_y(x, y), \quad (8)$$

$$v_x(-x, y) = v_x(x, y), \quad v_y(-x, y) = -v_y(x, y). \quad (9)$$

This configuration is also the starting point for the $\mathcal{R} \neq 0$ time-dependent problem, Eq. (1), to be treated hereafter.



$$\begin{aligned} \frac{\partial \omega}{\partial t} = & \frac{1}{\mathcal{R}\Delta^2} (\omega_1 + \omega_2 + \omega_3 + \omega_4 - 4\omega) \\ & - \frac{\omega_3 - \omega_1}{512\Delta} [81 (v_{xa} + v_{xb} + v_{xc} + v_{xd}) \\ & - 9 (v_{xe} + v_{xf} + v_{xg} + v_{xh} \\ & + v_{xi} + v_{xj} + v_{xk} + v_{xl}) \\ & + v_{xm} + v_{xn} + v_{xo} + v_{xp}] \quad (10) \\ & - \frac{\omega_2 - \omega_4}{512\Delta} [81 (v_{ya} + v_{yb} + v_{yc} + v_{yd}) \\ & - 9 (v_{ye} + v_{yf} + v_{yg} + v_{yh} \\ & + v_{yi} + v_{yj} + v_{yk} + v_{yl}) \\ & + v_{ym} + v_{yn} + v_{yo} + v_{yp}] \end{aligned}$$

Fig. 8. Discretized version of the Navier–Stokes dynamic Eq. (1).

From the current \vec{v} and ω distributions one determines the time derivative of ω through Eq. (10). With this, ω is updated as

$$\omega(t + \Delta t) = \omega(t - \Delta t) + 2\Delta t \frac{\partial \omega}{\partial t}, \quad (11)$$

where Δt is the discretized time interval adopted. In dimensionless units, we used $\Delta t = \Delta/10$. Not only $\omega(t)$ must be stored, but also $\omega(t - \Delta t)$ as well. This way, the whole procedure is second-order accurate also in time, i.e. the errors accumulated each new time step are proportional to the squared time interval Δt^2 . Once obtained the updated ω one determines the updated \vec{v} through Eq. (7), repeatedly applied until convergence.

Finally, ω must be relaxed until convergence through

$$\omega = \frac{\omega_1 + \omega_2 + \omega_3 + \omega_4}{4} - \mathcal{R}\Delta^2 \left\{ \frac{\partial \omega}{\partial t} + \frac{1}{2\Delta} [v_x(\omega_3 - \omega_1) + v_y(\omega_2 - \omega_4)] \right\}, \quad (12)$$

where v_x and v_y are the averages over points a, b, c and d in Fig. 8, passing by recalculations of \vec{v} through Eq. (7), as well as ω and $\partial \omega / \partial t$ through Eqs. (6) and (10), respectively, until complete convergence of both ω and \vec{v} fields.

After each time step one can follow the time evolution of \vec{v} and ω over the grid. Symmetry (8) remains for not so high Reynolds numbers, but symmetry (9) is broken for any $\mathcal{R} \neq 0$: The disturbed region behind the cylinder becomes longer than the

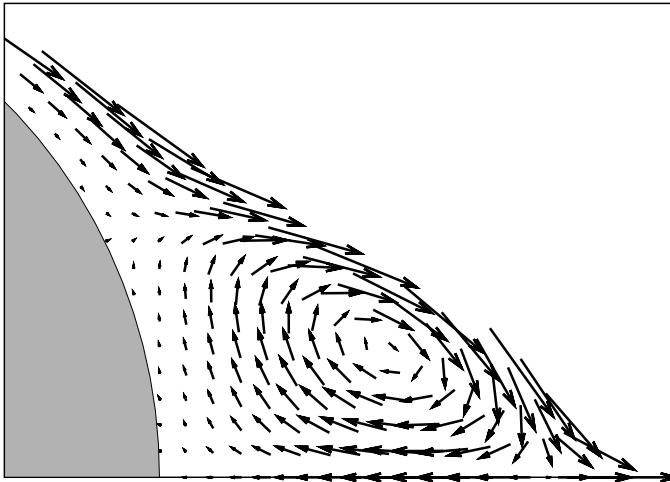


Fig. 9. Stationary steady-state reached after a certain transient time, for $\mathcal{R} = 30$. Only a small region behind the (gray) cylinder and above the X axis is shown. Symmetry (8) still holds, the other symmetric vortex runs counterclockwise below X , not shown. Arrows represent local velocities which are relatively small in this region. Speeds larger than 0.3 (relative to the wind speed) are omitted in the right upper corner of the figure.

front one, different from Fig. 7. For very small $\mathcal{R} \approx 1$, the flux remains laminar in spite of this asymmetry. For $\mathcal{R} \approx 10$ two symmetric air vortices appear behind the cylinder, one above the X axis running clockwise, the other below X running counterclockwise, thus preserving symmetry (8). Both vortices form simultaneously very near the cylinder, then they grow and move a little bit to the right. Finally they stabilize and remain at rest behind the cylinder, i.e. the whole field \vec{v} remains constant after some transient time. This steady-state is shown in Fig. 9 for $\mathcal{R} = 30$.

By increasing further the Reynolds number to $\mathcal{R} > 10^2$, no stationary steady state is reached, the flow becomes eternally time-dependent. The von Kármán street starts to be constructed. For $\mathcal{R} = 1000$, Fig. 10 shows an early stage in this evolution. Two still symmetric vortices have already appeared behind the cylinder, one of them is shown in the close up. Some time later, they have already moved a little bit downstream and start to become stretched along the X direction, as shown in Fig. 11. The slow movement downstream continues after that, as well as the stretching process.

Suddenly, too much stretched and some three or four diameters far from the cylinder, one vortex bifurcates and becomes a pair of vortices running in the same sense and repelling each other along the X direction. Symmetry (8) was finally broken, the other side remains with a single vortex for a while. Later on, it also bifurcates. Only then the von Kármán street begins to be formed: One vortex running clockwise slowly goes away downstream, followed by another running counterclockwise and so on. First, they are produced by bifurcations. Later, new vortices are produced in series near the cylinder back surface. Therefore, the complete street, extending some hundred diameters long, spends some time to be formed.

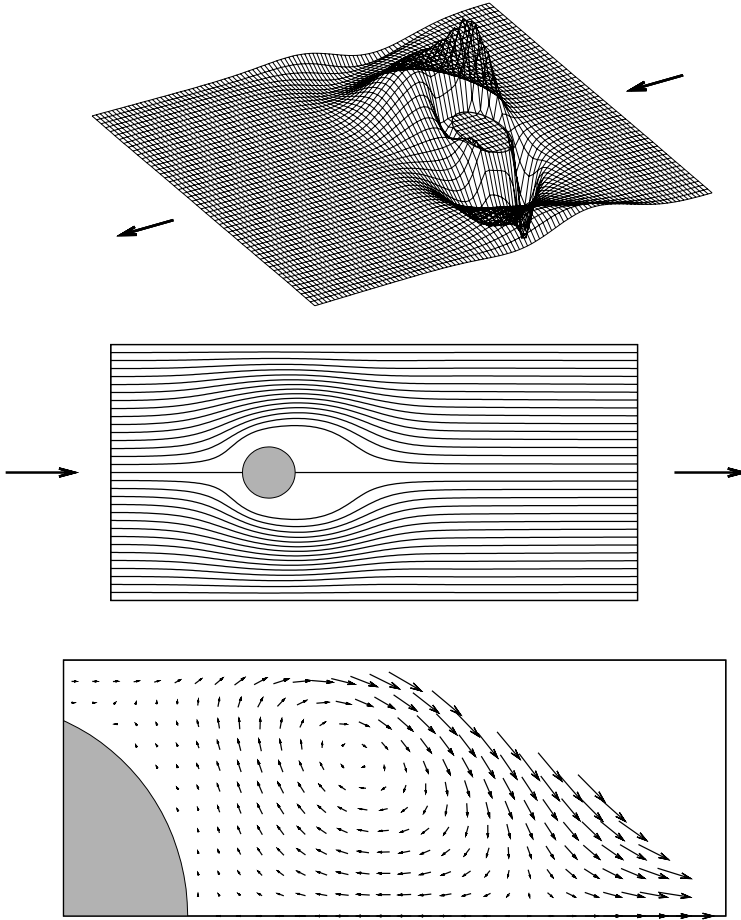


Fig. 10. Starting from the Stokes configuration (Figs. 6 and 7), the wind is switched on at $t = 0$ with a fixed Reynolds number $\mathcal{R} = 1000$. Figures show the result at $t = 1$, when a fluid element far from the cylinder has already travelled one diameter. The bottom figure is a close up of the region behind the cylinder, above the X axis, the other symmetric vortex below is not shown.

Two technical details remain to be explained. First, in order to avoid strong numerical fluctuations, after each time step a small fraction of the so-called numerical viscosity is introduced into the ω field. This procedure is traditional, consists in replacing ω by the combination $f \nabla^2 \omega + (1 - f)\omega$. In our $\mathcal{R} = 1000$ calculations, for instance, we adopted $f = 0.01$. Probably this step becomes unnecessary by using implicit integration methods, but again we decide to postpone performance improvements. Second, the rectangular frame $L_x \times L_y$ in Fig. 2 is not long enough to observe the complete von Kármán vortices street. Its length L_x is only 10 times larger than the cylinder diameter (three ahead and seven downstream). This is not a problem because our interest is only to observe the beginning of the street formation, i.e. the few first vortex bifurcations which occur some three or four diameter

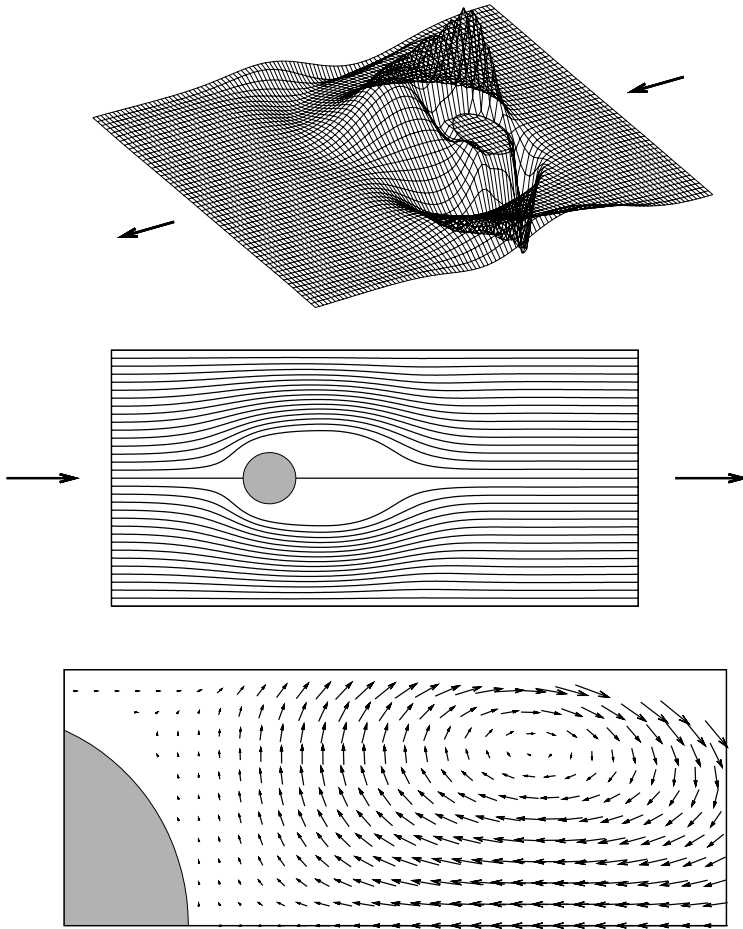


Fig. 11. Later than Fig. 10, $t = 2$. Vortices are still symmetric.

downstream. After that, the slowly moving vortices would be somehow “reflected” by the rigid boundary conditions adopted at the rightmost rectangle limit in Fig. 2, the back door. Nevertheless, by applying a simple trick, we could avoid this artificial behavior in order to observe forever the continuous vortex productions near the cylinder. For that, we change a little bit the boundary condition at the back door, as follows. Instead of keeping the rigid condition $\vec{v} = \hat{x}$, after each time step we replace it by the combination $f(y)\vec{v}(y) + [1 - f(y)]\hat{x}$, where $\vec{v}(y)$ are the velocities along the left neighbor column (the one just before the back door) and $f(y) = 1 - 2|y|/L_y$ (the rectangle width L_y in Fig. 2 corresponds to five cylinder diameters). This trick allows the vortices to escape through the back door, instead of being “reflected” back into the region near the cylinder.

The method can be easily applied to 3D systems, of course with some extra computer work due to a genuine 3D vector field $\vec{\omega}$. Before that, many improvements can

be introduced. One of them is to adopt another grid, not the square one of Fig. 2. For instance, a cylindrical grid with logarithmic scale in the radial direction. Another improvement is to control the number of relaxations up to convergence, within each time step (here, we simply fixed this number far above the necessary). Also, the convergence is not uniform, one can stop the relaxation process in regions already converged far from the cylinder, continuing the process further only near the cylinder.

3. Conclusions

This text introduces a relaxation method to solve the dynamical Navier–Stokes equation for not compressible fluids. It is applied to the flow past a long cylinder positioned inside a wind tunnel, perpendicular to the wind. The interest is the dynamic behavior during the transient time when the von Kármán street of vortices starts to be formed. The wind is initially switched off, therefore the starting velocity field is the laminar, time-independent Stokes configuration corresponding to a vanishing Reynolds number, without vortices. Then, at $t = 0$ the wind is switched on with some finite value \mathcal{R} of the Reynolds number. For $t > 0$ one can observe the gradual appearance of vortices near the cylinder, in sequence, which will eventually produce the quoted street. At the end, the street is known to extend downstream for some hundred diameters long.

The method was invented in order to observe the transient, during which the street is not yet completely formed and the drag force on the cylinder is strongly reduced when compared with the final steady state regime. This feature explains a curious experimental observation,⁴ in which a small and light polystyrene ball falling in air has its speed reduced. First, during the transient, the ball reaches a larger speed. Later, when the von Kármán vortices street is finally complete and the drag force reaches its steady state, the speed is reduced to the final sustainable value. A similar and equally curious phenomenon is also observed⁷ during the transient when the wake gradually forms: The speed of a light and small ball falling in water oscillates. The authors speculate about new unexpected phenomena to be observed for lighter and smaller yet balls. We can add some kind of hysteresis and eventual bistability with two possible final speeds.

“This text is dedicated to David Landau. Would he read it, I can imagine his question about the contents, with his loud voice: ‘... What about the error bars?’ I could not introduce error bars into my figures showing the simulated air flow, but at least beautiful error bars can be seen in the experimental plot, Fig. 1. Congratulations to David.”

Acknowledgments

I am indebted to an anonymous referee who drives my attention to the related problems presented in Ref. 5 and helpful comments. Also to Suzana Moss de Oliveira for a critical reading of the final text and suggestions.

References

1. E. M. Purcell, *Berkeley Physics Course*, Chap. 38, Vol. 2 (MacGraw-Hill, New York, 1965).
2. R. P. Feynman, *The Feynman Lectures on Physics*, Chap. 41, Vol. 2 (Addison-Wesley, Reading, MA, 1965).
3. M. J. Wright, G. V. Candler and D. Bose, *AIAA J.* **36**, 1603 (1998).
4. P. M. C. de Oliveira, S. Moss de Oliveira, F. A. Pereira and J. C. Sartorelli, preprint (2010), arXiv:1005.4086.
5. L. D. Landau and E. M. Lifshitz, *Fluid Mechanics*, 2nd edn. (Pergamon, Oxford, 1987).
6. C. Peruzzi, <http://peruzzic.files.wordpress.com/2010/07/falling031.pdf> (2010).
7. M. Mordant and J.-F. Pinton, *Eur. Phys. J. B* **18**, 343 (2000).